Identification of select G-protein coupled receptors as regulators of the ER-mitochondria contact by drug screening

Youngshin Lim[1#], Il-Taeg Cho[1#, 2], Helmut G. Rennke[1], and Ginam Cho[1*]

From the [1]Department of Pathology, Brigham and Women's Hospital and Harvard Medical School, Boston, MA 02115, USA.

Running title: Drug screen for ER-Mito contact enhancers

[2] Present address: Department of Surgery, Keck School of Medicine, University of Southern California, Los Angeles, CA 90033, USA.

[#] Equal contribution

[*] To whom correspondence should be addressed: gpcho@bwh.harvard.edu

Keywords: β-adrenergic receptors (β-ARs), β-AR agonists, calcium, cAMP, endoplasmic reticulum-mitochondria contact, drug screen, G-protein coupled receptors (GPCRs), GPCR agonists, split-Rluc reassembly assay.

ABSTRACT

Endoplasmic reticulum-mitochondrial (ER-Mito) contacts are crucial for many cellular functions. Their dysregulation has been implicated in many disorders including neurodegenerative, cardiovascular and metabolic diseases, and cancer. However, little is known about the regulatory pathways of ER-Mito contacts. To uncover such pathways, we screened a drug library for the ER-Mito contact modulators using a split-luciferase reassembly assay. We identified multiple agonists of G-protein coupled receptors (GPCRs), beta-adrenergic receptors (β-ARs) in particular, in our screen. Using multiple independent assays, we validated that these drugs enhance the physical and functional interactions between ER and mitochondria. Our data provide evidence that cytoplasmic calcium plays a role in drug-induced ER-Mito coupling. Together our study identifies GPCR activation as a novel regulatory mechanism of ER-Mito contacts and highlights the role of these contacts in responding to physiological demands or stresses. Furthermore, our findings reveal a new mechanism of action for β-AR agonists in multiple diseases.

INTRODUCTION

In eukaryotic cells, membrane-bound organelles accomplish specialized functions in isolated compartments. For these organelles to communicate with each other, they use either vesicular trafficking system requiring membrane fusion, or membrane contact sites where the membranes of interacting organelles become closely juxtaposed without fusion. Despite the fact that they have emerged only recently as a matter of interest when compared to vesicular trafficking system, the membrane contact sites have been extensively studied in recent decades (Rowland & Voeltz 2012; Csordás et al. 2018; Scorrano et al. 2019).

ER-mitochondria (ER-Mito) contact is one of the most studied inter-organelle interaction (Klecker et al. 2014; Phillips & Voeltz 2016; Csordás et al. 2018; Tepikin 2018). In yeast, this contact is primarily tethered by the ER-mitochondria encounter structure (ERMES) complex that consists of four proteins (Mdm12, Mmm1, Mdm34, Mdm10) (Kornmann et al. 2009; Lang et al. 2015). Similar contacts have been identified in mammalian cells, although their molecular identity is much more complicated and still debated (Eisenberg-Bord et al. 2016; Kornmann 2013; Lee & Min 2018). The function of the ER-Mito contact sites includes the transfer and metabolism of lipids (Vance 2014; Vance 1990); modulation of Ca^{2+} fluxes and homeostasis (Rizzuto et al. 1993; Rizzuto et al. 1998); formation of dynamic H_2O_2 nanodomains that regulate Ca^{2+} signaling (Booth et al. 2016); control of mitochondria fusion-fission dynamics (de Brito & Scorrano 2008; Friedman et al. 2011); biogenesis of autophagosomes and mitophagosomes (Hamasaki et al. 2013; Böckler & Westermann 2014); and control of apoptosis (Simmen et al. 2005). The failure to maintain normal ER-Mito contacts has emerged as a common hallmark of multiple human diseases (e.g., neurodegenerative, cardiovascular and metabolic diseases, and

cancer) (Paillusson et al. 2016; Moltedo et al. 2019; Rieusset 2018; Doghman Bouguerra & Lalli 2019). For example, we have shown that the disease-associated mutations in REEP1, which are linked to hereditary spastic paraplegia (whose cardinal feature is weakness and stiffness in the leg muscles due to neurodegeneration), result in reduction in ER-Mito contacts compared to wild type REEP1(Lim et al. 2015).

Although significant work remains, multiple studies suggest that both abnormal increases and decreases in ER-Mito contacts are detrimental to normal cellular functions (Paillusson et al. 2016). If ER-Mito contacts are abnormally enhanced, as observed in some Alzheimer's disease models (Tambini et al. 2016; Area-Gomez et al. 2012; Hedskog et al. 2013; Zampese et al. 2011), it has been postulated that the resulting mitochondrial Ca^{2+} overload would cause mitochondrial permeability transition pores (mPTP) to open, and eventually leading to mitochondrial swelling and cell death (Tepikin 2018). On the other hand, if the contacts are abnormally reduced or disrupted, as in the cases of amyotrophic lateral sclerosis with associated frontotemporal dementia (ALS/FTD) models (Stoica et al. 2014; Stoica et al. 2016; Watanabe et al. 2016; Lau et al. 2018), the decreased contact is predicted to lower mitochondrial ATP generation (Tepikin 2018), which in turn would drive motor neuron degeneration as shown in a recent study (Le Masson et al. 2014). Despite their implication in many diseases and the importance of maintaining their normal level in the cell, little is known about how ER-Mito contacts are regulated.

We previously developed a split-*Renilla* luciferase (split-Rluc) reassembly assay to quantitatively measure the level of physical coupling between ER and mitochondria (Lim et al. 2015; Cho et al. 2017). Our split-Rluc system consists of two separate DNA constructs, one encoding the split-half of the *Renilla* luciferase with a mitochondrial targeting sequence (Mito-$Rluc^{N}$) and the other encoding the other half with an ER targeting sequence ($Rluc^{C}$-ER) (Lim et al. 2015).

While each construct by itself cannot generate luciferase activity, co-expression of both constructs results in full enzymatic activity at the ER-Mito contact sites where the two halves are close enough to reassemble and restore the luciferase activity. Although there are several established methods to detect ER-Mito contacts in cells (Csordás et al. 2018; Scorrano et al. 2019), our split-Rluc reassembly assay is optimal for drug screening, as it permits high throughput detection of the ER-Mito contacts in live cells without artifacts associated with sample fixation or complications related to image analysis.

Using this split-Rluc assay in HEK293T cells, we screened an NIH clinical collection (NCC) of FDA approved drugs to identify compounds that could potentially enhance ER-Mito contacts. All 11 positive hits were agonists of G-protein coupled receptors (GPCRs) and 9 of them target beta-adrenergic receptors (β-ARs). Our data reveal for the first time that GPCRs, and β-ARs in particular, act as a major regulatory signaling for ER-Mito contacts. Given the role of GPCRs in sensing various extracellular signals (e.g., photons, ions, lipids, amines, peptides, growth factors, and hormones) (Neumann et al. 2014) and subsequently eliciting appropriate cellular responses, our data provide significant insights into the roles of ER-Mito contacts in maintaining cellular homeostasis and in responding to physiological demands (or stresses) such as increases in mitochondrial ATP generation, alteration in lipid production, and/or autophagy induction.

RESULTS

Screening FDA approved drugs for ER-Mito contact enhancers using split-RLuc reassembly assay.

To identify compounds that enhance ER-Mito contact, we screened a library of 720 FDA-approved investigational drugs (NIH Clinical Collection, NCC) with the split-Rluc reassembly assay (Fig. 1) (Lim et al. 2015; Cho et al. 2017). HEK293T cells expressing split-Rluc constructs were treated with DMSO (control) or each drug at 1 μM final concentration for 5 hours (Fig. 1A, B). The luciferase activity in live cells was measured using EnduRen™ as a substrate and normalized by the quantile method (Bolstad et al. 2003). From the initial screen, we identified 32 potential hits (4.4% hit rate) using the cut-off value of 3 standard deviation (SD) above the average of the control (Fig. 2A; Table S1). These potential hits were found to target G-protein coupled receptors (GPCRs) (18 drugs, 56% of 32); glucocorticoid receptors (5 drugs, 16% of 32; labeled as steroid); DNA topoisomerases/polymerases (5 drugs, 16% of 32; labeled as DNA related); and ion channels/transporters (2 drugs, 6% of 32; labeled as ion channels) (Fig. 2B; Table S1). NCC library contains 331 (46% of 720 drugs) annotated drugs associated with GPCR pathways according to our manual curation (Table S2) based on the information available from PubChem (https://pubchem.ncbi.nlm.nih.gov). Among the potential hits linked to GPCRs, the majority of them (11 drugs, 61% of 18) are found to target ARs (Fig. 2B; Table S2). Considering that only 17% (59 of 348) of GPCR-associated drugs in this library target ARs (Fig. 2C; Table S2), these data indicate an enrichment of AR-associated drugs in our initial screen.

To exclude potential false positives, we repeated the split-Rluc assay with these 32 drugs and confirmed positive results for 16 compounds (Fig. 3A, B). Of note, the effect of these drugs on split-Rluc protein expression level was comparable with a small variation (data not shown). Out of 16 confirmed compounds, 11 drugs exhibiting 3 times or greater activity than DMSO are referred to as 'hits' in our screen, and all of them are GPCR agonists: nine of them target ARs

and the other two, alprostadil (a.k.a. prostaglandin E1, PGE1) and 2-chloro-N^6cyclopentyladenosine (CCPA), target prostaglandin and adenosine receptor pathways, respectively (Fig. 3B). Notably, all nine of the AR agonists showed stronger activity compared to PGE1 and CCPA (Fig. 3A, B). Among these nine agonists, seven of them are specific for β-ARs, while the other two, epinephrine and norepinephrine, activate both α- and β-ARs. Isoproterenol (a.k.a. isoprenaline), metaproterenol, and duvadilan are non-selective β-AR agonists, while terbutaline, salmeterol, formoterol, and salbutamol are specific to β2-AR (Fig. 3B) (https://pubchem.ncbi.nlm.nih.gov/). NCC library contains 59 (8% of 720) annotated compounds associated with AR pathway (Fig. 3C; Table S3) and we found that all 9 hits annotated to AR pathway are agonists of β-ARs (epinephrine and norepinephrine activates both α- and β-ARs), while all other compounds (not identified as hits) are either agonists/antagonists of α-ARs or antagonists of either β-ARs or of both α- and β-ARs (Fig. 3C; Table S3). These findings point out that our screen successfully identified only specific drugs that can activate β-ARs among other AR associated drugs. Taken together, these data indicate that the activation of GPCRs, especially β-ARs, likely play a key role in modulating ER-Mito contacts.

Next, to validate the increase in split-RLuc activity is not exclusively the result of enhanced split-Rluc expression, we measured the effect of the selected drug (isoproterenol) with or without the transcription inhibitor actinomycin D (Fig. 3D). In cells treated with actinomycin alone, split-Rluc activity was lowered (suggesting some ER-Mito contact is in part influenced by transcription inhibition). However, isoproterenol treatment significantly lifted the inhibitory effect of actinomycin (Fig. 3D), indicating that the isoproterenol-induced split-Rluc activity indeed resulted from the elevated level of the physical tethering between the two organelles and not as a result of increased gene expression alone. Of note, all subsequent studies were

performed targeting less than two to three-fold increase in luciferase activity upon isoproterenol treatment to minimize potential damages from high levels of ER-Mito contacts.

GPCR agonists, isoproterenol, CCPA, and PGE1, increase physical contact between ER and mitochondria.

As noted above, three classes of hits were identified among the 720 compounds. We selected one member from each class to further investigate a potential role in ER-Mito contacts; isoproterenol is a β-AR agonist (https://pubchem.ncbi.nlm.nih.gov/compound/3779) and was selected out of the nine AR agonist hits because it showed the strongest effect (Fig. 3B), CCPA is a specific agonist for the adenosine A1 receptor (https://pubchem.ncbi.nlm.nih.gov/compound/123807), and PGE1 is specific for the prostaglandin E2 receptor subtypes EP1 and EP2 (https://pubchem.ncbi.nlm.nih.gov/compound/5280723).

In order to corroborate our split-Rluc assay results and validate that the selected drugs can indeed enhance physical contact between ER and mitochondria, we employed two independent assays. First, we used an *in situ* proximity ligase assay (PLA), which is based on the labeling of two proteins present in close proximity in fixed cells with specific primary antibodies and oligonucleotide-linked secondary antibodies (Söderberg et al. 2006). Primary antibodies against ER protein SEC61-GFP and mitochondrial protein TOM20 were selected. When SEC61 and TOM20 are in sufficient proximity (i.e., ER-Mito contact is formed), subsequent ligation and rolling circle amplification reactions lead to a fluorescent product (red) that can be detected *in situ* (Fig. 4A). We found that the PLA fluorescence signal from the cells treated with these drugs

were significantly higher than those treated with DMSO (control), supporting that these drugs indeed raise ER-Mito contacts (Fig. 4A, B).

Next, we assessed ER-Mito contact at the ultrastructural level by transmission electron microscopy (TEM). HEK293T cells treated with DMSO or isoproterenol for 30 min were fixed and processed for TEM, and electron micrographs were used to determine the extent of ER-Mito contacts. The percentage of mitochondria juxtaposed (< 30 nm) to ER in isoproterenol treated cells was higher than in DMSO treated cells (DMSO, 22%; isoproterenol, 38%) (Fig. 4C, D), thus again corroborating our results with split-Rluc assay.

GPCR agonists, isoproterenol, CCPA, and PGE1, enhance functional coupling between ER and mitochondria.

We next asked if the drug-induced physical contact between ER and mitochondria created functional coupling between these organelles. Given the previous studies that established the ER-Mito contact sites as hotspots for Ca^{2+} influx to mitochondria (Rizzuto et al. 1993; Giacomello et al. 2010; Tepikin 2018), we investigated if the drug treatment could increase mitochondrial Ca^{2+} influx. To quantify Ca^{2+} levels in the mitochondria, we utilized a fluorescent Ca^{2+} sensors, mito-R-GECO1 (Wu et al. 2013; Zhao et al. 2011). HeLa cells were treated with DMSO or one of the three drugs for 4 hours: isoproterenol, CCPA, and PGE1. Mitochondrial Ca^{2+} uptake was then measured in response to histamine-stimulated ER Ca^{2+} release every 2.5 seconds (Fig. 5A). Upon ER Ca^{2+} release, all three drugs, compared to DMSO, resulted in a higher maximum peak (Fig. 5A, B) and faster uptake rate (Fig. 5A, C) of mitochondrial Ca^{2+}. These data suggest that they triggered elevated and accelerated mitochondrial Ca^{2+} responses when compared to control.

Thus, these drugs increased not only physical but also functional coupling between ER and mitochondria. Furthermore, consistent with the physical contact data (Fig. 3B), isoproterenol appears to be more potent than CCPA or PGE1 in functional coupling, given the highest level of its effect on ER-to-mitochondrial Ca^{2+} transfer (Fig. 5A-C).

Several lines of evidence indicate that ER-Mito contact contributes to mitochondrial bioenergetics by supplying Ca^{2+} to mitochondria (Filadi et al. 2018; Bravo et al. 2011; Cárdenas et al. 2010; Tepikin 2018), because proteins involved in Krebs cycle and oxidative phosphorylation can be activated by Ca^{2+} (Balaban 2009; Territo et al. 2000; Cárdenas et al. 2010; Denton 2009). Accordingly, we next investigated if facilitated Ca^{2+} uptake by drug treatment would increase mitochondrial bioenergetics. For this purpose, we measured mitochondrial membrane potential (Fig. 5D, E) and mitochondrial DNA content (Fig. 5F), indicators of increased mitochondrial metabolism and health (Perry et al. 2013). Tetramethyl rhodamine methyl ester (TMRM) fluorescence dye was used to determine mitochondrial membrane potential (Scaduto & Grotyohann 1999) and mitochondrial DNA content was measured by PCR (Rooney et al. 2015). We found increases in mitochondrial membrane potential (Fig. 5E) as well as mitochondrial DNA content, in isoproterenol treated cells (Fig. 5F). These findings imply that drug-induced ER-Mito contacts lead to enhanced mitochondrial metabolism via facilitated ER-to-mitochondria Ca^{2+} transfer.

PKA inhibition does not abolish βAR agonist-induced ER-Mito contact

βAR activation, similar to activation of other GPCRs, usually leads to an intracellular production of cAMP via adenylate cyclase, resulting in the activation of protein kinase A (PKA)

which in turn regulates multiple downstream proteins via phosphorylation (Fig. 6A) (Ciccarelli et al. 2013). To determine if this cAMP/PKA pathway is involved in agonist-induced ER-Mito contact modulation, we treated cells with the PKA inhibitors, Rp-cAMPS and H-89, together with DMSO or isoproterenol. We found that the PKA inhibitors failed to abolish the positive effects of isoproterenol on ER-Mito contact (Fig. 6B), indicating that the cAMP/PKA pathway does not play a role in isoproterenol-mediated ER-Mito contact enhancement in our system. Furthermore, increasing cAMP level by forskolin treatment did not change ER-Mito contact level either (Fig. 6C). Taken together these data suggest that cAMP/PKA pathway is not the main pathway through which isoproterenol-mediated βAR activation modulates ER-Mito contact.

Elevated cytosolic calcium concentration enhances ER-Mito contact level.

Since we found no evidence that isoproterenol signaled through the cAMP/PKA pathway to ER-Mito contacts, we next investigated if cytoplasmic Ca^{2+} levels, another second messenger of the βAR pathway, would affect juxtaposition of ER and mitochondria. For this purpose, we assessed the split-Rluc activity in the cells treated with histamine, ionomycin or cyclopiazonic acid (CPA), all of which are known to raise cytosolic calcium by distinct mechanisms (Chakrabarti et al. 2018; Plenge-Tellechea et al. 1997). Histamine stimulates cytosolic Ca^{2+} release from the ER (Chakrabarti et al. 2018); ionomycin, a membrane permeable Ca^{2+} ionophore, enhances extracellular Ca^{2+} influx to the cytoplasm (Chakrabarti et al. 2018); and CPA, a sarco-endoplasmic reticulum Ca^{2+}-ATPase (SERCA) inhibitor, blocks the uptake of Ca^{2+} ions back to the sarcoplasmic reticulum (SR)/ER lumen after their release into the cytosol, thus

accumulating Ca^{2+} in the cytoplasm (Plenge-Tellechea et al. 1997). All three drugs elevated the luciferase activity (Fig. 7A), indicating that the upregulation of cytoplasmic Ca^{2+} concentration is sufficient to enhance ER-Mito contacts (of note, thapsigargin, another SERCA inhibitor, did not enhance luciferase activity (data not shown), although at present we do not have an explanation why). Our findings with the split-Rluc assay were corroborated using *in situ* PLA. Upon histamine or ionomycin treatment, PLA fluorescence signal was increased when compared to DMSO control (Fig. 7B).

Previous reports indicate that multiple stimuli leading to increased cytosolic Ca^{2+}, such as ionomycin and histamine, trigger a transient surge in cytosolic actin polymerization that enhances ER-Mito contacts (Ji et al. 2017; Shao et al. 2015; Chakrabarti et al. 2018). Therefore, we hypothesized that an actin polymerization 'burst' would be required for isoproterenol-induced ER-Mito contact. To test this hypothesis, we investigated if changes in ROCK activity, which is under GPCR signaling and involved in actin polymerization (N. Mittal et al. 2013), would alter the level of physical contact between ER and mitochondria. For this purpose, we treated HEK293T cells with ROCK inhibitor, Y-27632, and measured the split-Rluc activity. Y-27632 treated cells showed lower luciferase activity than DMSO treated ones (Fig. 7C), suggesting a decreased ER-Mito contact likely due to impaired actin polymerization.

Further evidence supporting the positive influence of actin polymerization on ER-Mito contact comes from our study with *Cdc42* expression (Fig. 7D). CDC42 is a member of the Rho family of small GTPases and plays important roles in actin polymerization; GPCR signal is one of the various upstream signals for CDC42 activation (Sinha & Yang 2008). To examine the effect of CDC42 activation or inhibition on ER-Mito contacts, we co-transfected wild type *Cdc42* (Cdc42 WT), constitutively active *Cdc42* (Cdc42 CA), or dominant negative *Cdc42*

(Cdc42 DN) construct together with split-Rluc constructs (Cdc42 CA is known to enhance actin polymerization, while Cdc42 DN disrupts polymerization (Johnson 1999). Cdc42 CA expressing cells showed significantly higher luciferase activity than the control vector or Cdc42 WT expressing cells, whereas Cdc42 DN expressing cells showed lower activity although it did not reach statistical significance (Fig. 7D). These results provide further evidence that actin polymerization, likely achieved through increased cytosolic Ca^{2+}, may play a role in ER-Mito contact upregulation by βAR activation.

Given previous studies showing that myosin IIA contributes to actin-mediated enhancement of mitochondrial Ca^{2+} influx (Chakrabarti et al. 2018), we next tested the effect of blebbistatin, a myosin II inhibitor that prevents actomyosin cross-linking, on ER-Mito contact formation. HEK293 cells treated with blebbistatin demonstrated a dose-dependent decrease in split-Rluc activity (Fig. 7E), supporting that actomyosin cross-linking positively affects ER-Mito contacts. This finding is in line with the previous reports that suggested myosin II may provide 'contractile tension' for ER-Mito contact (Chakrabarti et al. 2018).

Finally, we asked if microtubule polymerization is also involved in ER-Mito contact modulation, given that mitochondria move along microtubules, and that mitochondrial motility has been proposed to affect ER-Mito contact (Yi et al. 2004). Surprisingly, HEK293 cells treated with nocodazole, a drug that interferes with microtubule polymerization, showed a dose-dependent increase in split-Rluc activity (Fig. 7F). This result raises a possibility that forced arrest of mitochondrial movement due to impaired microtubule polymerization might increase the chance of ER-Mito interaction. In line with this result, increased cytosolic calcium has been shown to arrest mitochondrial movement along the microtubule (Yi et al. 2004). Although further investigation is required, our data with cytoskeletal reagents support the notion that the

inter-organelle interaction is facilitated by actin assembly, but also their coupling may be hindered by excess organelle dynamics along microtubule (Moore & Holzbaur 2018; Yi et al. 2004).

DISCUSSION

Communication between the ER and mitochondria is crucial for many cellular functions. Although recent studies have focused on the molecular components of these contacts, the regulatory pathways of ER-Mito contacts remain largely unknown. In this study, we have made the novel discovery that select GPCRs, β-ARs in particular, are significant regulators of ER-Mito interactions. Given that the GPCR pathway senses the extracellular/environmental signals and modulates appropriate cellular responses, our findings indicate that ER-Mito contacts provide an important link between extracellular stimuli (environmental changes) and intracellular responses. For instance, when agonist-induced GPCR signaling enhances ER-Mito contacts, ER-to-mitochondrial Ca^{2+} transfer is facilitated, thus activating mitochondrial matrix proteins to generate more ATP (Denton 2009; Bravo et al. 2011).

GPCRs transduce their signals through G proteins consisting of three subunits, G_{α}, G_{β}, and G_{γ}. Upon GPCR activation, G_{α} can dissociate from G_{β} and G_{γ} subunits to affect other molecules in the cell depending on its subunit type ($G_{\alpha s}$, $G_{\alpha i/o}$, $G_{\alpha q/11}$, $G_{\alpha 12/13}$) (Neumann et al. 2014; Inoue et al. 2019). $G_{\alpha s}$ relays a signal to adenylate cyclase to generate cAMP whose level determines the activity of PKA family (as well as various ion channels). $G_{\alpha i/o}$ works in a negative way to inhibit adenylate cyclase. On the other hand, the effector of $G_{\alpha q/11}$ is phospholipase C_{β} (PLC_{β}) which cleaves PIP2 into IP3 and DAG, to elicit calcium release from ER. Finally, the effectors of

$G_{\alpha 12/13}$ are RhoGEFs which activate small GTPase, Rho. GTP-bound Rho can activate various proteins responsible for cytoskeleton regulation such as Rho kinase (ROCK). In addition, it is known that GPCRs can also signal through G-protein-independent mechanisms via proteins such as β-arrestin (Billington et al. 2017). According to our data with cAMP-RP and E89 (PKA inhibitors), isoproterenol-induced ER-Mito contact appears to be independent of PKA pathway activation. Despite this observation, we cannot rule out the possibility that cAMP may still be involved, considering that cAMP can activate other downstream effectors such as a small family of guanine nucleotide exchange factors (GEFs) (e.g., exchange protein activated by cAMP, EPAC) (de Rooij et al. 1998). However, given no effect of forskolin (adenylate cyclase activator) on ER-Mito contact in our PLA, it is more likely that the non-canonical GPCR pathway via β-arrestin-2, rather than cAMP pathway, may play a role in β-AR activated ER-Mito contact. Consistent with this model, low concentrations of β2-AR agonist (salmeterol) have been shown to act through the β-arrestin-2 pathway, not utilizing cAMP/PKA or cAMP/Epac pathway, when exerting its anti-inflammation effect (Qian et al. 2011).

Unlike cAMP, increased cytosolic Ca^{2+}—whether resulting from increased entry through the plasma membrane (by ionomycin), increased release from ER (by histamine), or depleted ER storage (by CPA)—appears to trigger the coupling between the ER and mitochondria. In addition to its effect on actin polymerization that facilitates ER-Mito juxtaposition, increased cytosolic Ca^{2+} might exert its effect through mitochondria motility control, given that increased cytosolic Ca^{2+} has been shown to arrest mitochondrial movement along the microtubule (Yi et al. 2004). Paused mitochondrial movement increases the likelihood of its interaction with ER (Yi et al. 2004). Consistent with this, when the split-Rluc activity was measured in the presence of nocodazole (inhibitor of microtubule polymerization thus blocking mitochondrial motility), ER-

Mito contact was increased (Fig. 7F). Of note, when the cut-off threshold is lowered to 2SD instead of 3SD in our initial screen, flubendazole, a tubulin inhibitor, is among the potential hits that enhance ER-Mito contacts (Table S1), providing further evidence supporting the inverse relationship between the mitochondrial motility and the extent of chance of ER-Mito contacts. Finally, it is also possible that the increased cytosolic Ca^{2+} might 1) trigger activation of unknown regulatory molecules to enhance ER-Mito contacts, or 2) facilitate tethering complex formation independent of cytoskeletal dynamics. In line with the first possibility, previous work has shown that Miro, a mitochondrial Rho GTPase (involved in mitochondrial transport) with two Ca^{2+} sensing EF-hand domains, enhances functional coupling between ER and mitochondria in a manner likely independent of mitochondrial transport (Lee et al. 2016). Our data in conjunction with this study suggest that Miro could be a good candidate modulator of ER-Mito contacts that responds to the increased cytosolic Ca^{2+}(Lee et al. 2016). Moreover, in agreement with the second possibility, E-Syt1 (extended synaptotagmin 1), an ER protein that participates in ER- plasma membrane (PM) tethering, has been shown to require cytosolic Ca^{2+} increase for its tethering functions (Giordano et al. 2013), raising the possibility of such tethering protein(s) in ER-Mito contacts.

Accumulating evidences indicate that ER-Mito contact dysfunction contributes to a variety of neurodegenerative diseases including Altzheimer's disease (AD), Parkinson's disease (PD), amyotrophic lateral sclerosis with associated fronto-temporal dementia (ALS/FTD), Charcot-Marie-Tooth (CMT) disease and hereditary spastic paraplegia (HSP) (Moltedo et al. 2019; Paillusson et al. 2016; Joshi et al. 2016; Krols et al. 2016). For example, disease-associated mutations in presenilin1 and 2 in AD (Hedskog et al. 2013; Schon & Area-Gomez 2013; Filadi et al. 2016; Area-Gomez et al. 2012); α-synuclein (α-syn), DJ-1, PINK1 and parkin in PD (Calì et

al. 2012; Gelmetti et al. 2017; Barazzuol et al. 2020; Ottolini et al. 2013); SOD1 in ALS/FTD (Stoica et al. 2014); Mitofusin 2 in CMT (de Brito & Scorrano 2008); and REEP1 in HSP (Lim et al. 2015), have shown to alter ER-Mito contacts, with evidence suggesting this change contributes to the neurodegeneration. It is interesting to speculate on the possibility that the drugs we have identified (that physically and functionally enhance ER-Mito contacts) represent potential therapeutics for conditions such as PD, FTD/ALS, and HSP, where reduced ER-Mito contacts have been implicated in pathogenesis (Paillusson et al. 2016). Accordingly, agonists to β2-AR have been shown to be effective for PD therapy, although the mechanism has been attributed to their anti-inflammatory activity (Magistrelli & Comi 2020; Peterson et al. 2014). Furthermore, salbutamol and metaproterenol (β2-AR agonists), both of which were also identified in our screen, reduce α-syn transcription levels, and salbutamol was associated with a reduced risk of developing PD in Norwegians (Mittal et al. 2017). Although their efficacy was linked to α-syn transcription regulation (Mittal et al. 2017) and anti-inflammation (Qian et al. 2011), our data indicate that these drugs might also exert therapeutic effects by increasing ER-Mito contacts as some PD associated insults appear to disrupt these contacts (Barazzuol et al. 2020). Thus, our study suggests a new mechanism of action for β2-AR agonists that are currently used for treatment of PD and other diseases. Furthermore, this also offers potential therapeutic options for conditions shown to have a component of the disease process associated with disrupted ER-Mito contacts. When considering ER-Mito contact enhancement drugs for therapeutic options, however, it is important to recognize that both increased and decreased ER-Mito contacts can be detrimental. Therefore, careful titration of these drugs will be crucial.

In summary, we found that GPCR signaling, especially through β-ARs, is a significant regulator of ER-Mito contacts. Our data provide new insights into how changes in physiological

demands in the cell can signal to induce changes in ER-Mito contacts that elicit physiological responses. Furthermore, the results we present here indicate that our split-Rluc reassembly assay can serve as a valid assay to screen for modulators of ER-Mito contacts, although we recognize the likelihood of potential false negative hits due to its limitation with *in vitro* cell culture system. While our current screen focused on an FDA-approved drug library, further screens with other compound libraries (identifying small molecules that could target ER-Mito contact sites directly) will likely provide additional biologic insights into this important inter-organelle communication. Furthermore, ORF or siRNA library screens would be warranted to identify additional molecular machinery functioning for this contact. Finally, while our current screening system is most suitable for enhancer (or promoter) identification due to low basal level of split-Rluc activity, modification to our system could permit the screening for inhibitors of ER-Mito contacts in the future study.

Materials and methods

Plasmids and DNA constructs

Split-Rluc constructs in pcDNA3.1 (Mito-Rluc^{N} and Rluc^{C}-ER) have been described previously (Lim et al. 2015). pCMV-mito-R-GECO1 (plasmid #46021), pAAV.CAG.GCaMP6s.WPRE.SV40 (plasmid #100844), and pAc-GFPC1-Sec61β (plasmid #15108) were obtained from Addgene (gift from Robert Campbell, Douglas Kim & GENIE Project, and Tom Rapoport, respectively) (Wu et al. 2013; Chen et al. 2013; Voeltz et al. 2006). Wild type Cdc42 expression vector under CMV promoter (pcDNA3.1) was constructed by RT-PCR from E13.5 mouse embryonic brain tissue with primers 5'- CCGCCAGTGTGCTGG cacc atgcagacaattaagtgtgttgttgttggtgatggtg-3' and 5'- GATGCATGCTCGAGC tcatagcagcacacacctgcggctcttctt -3'. For constitutively active (CA) and dominant negative (DN) Cdc42, we introduced mutations at Q61L and T17NP (Johnson 1999), respectively by PCR. All clones were confirmed by sequencing.

Compounds and chemical reagents

We used NIH Clinical Collections 1 and 2 (NCC) (Evotec, San Francisco, CA) containing 720 FDA approved drugs dissolved in 100% DMSO at a concentration of 10 mM, for screening (note: the original list contains 727 drugs but 7 of them are duplicated). The target pathway(s) of the members of this collection was manually curated from the information available in the PubChem portal http://pubchem.ncbi.nlm.nih.gov/. For post-screen experiments, three GPCR agonists, isoproterenol (1747, Tocris), CCPA (119136, Sigma-Aldrich), and prostaglandin E1 (P5515, Sigma-Aldrich) were obtained from each indicated vendor and used at 1μM final concentration. For cAMP pathway related reagents, cAMPS-Rp (13371, Tocris), H89 (2910,

Tocris), and forskolin (F3917, Sigma-Aldrich) were used at a concentration of 10 μM, 10 μM, and 20 μM, respectively. To increase cytoplasmic calcium concentration, we used histamine (H7250, Sigma-Aldrich), ionomycin (1704, Tocris), and cyclopiazonic acid (CPA, C1530, Sigma-Aldrich) at a concentration of 100 μM, 1 μM, and 10 μM, respectively. Blebbistatin (B0560, Sigma-Aldrich), nocodazole (S2775, Selleck Chemicals), and 1 μM of Y-27632 (SCM075, EMD Millipore) were treated to investigate cytoskeletal rearrangement effects. For DMSO used as controls, the final concentration was decided according to the experimental drug's final concentration (e.g., 0.01% DMSO was used as a control, when other drugs (in 100 % DMSO) were used 1:10000 dilution).

Cell culture and transfection

HEK293T and HeLa cells were maintained in DMEM (Thermo Fisher Scientific) with 10% FBS (Thermo Fisher Scientific) in a humidified incubator at 37°C with 5% CO_2. For transfection with split-Rluc constructs, HEK293T cells (4 x 10^5 /well) were plated in a 12-well culture plate to obtain 75-80% confluency. After overnight culture, cells were transfected with indicated DNA constructs (400 ng each) using polyethylenimine (PEI; Polysciences, Eppelheim, Germany) as previously described (Lim et al. 2015; Cho et al. 2017).

Split-Renilla luciferase (split-Rluc) reassembly assay

HEK293T cells were transfected with split-Rluc reporter plasmids (Mito-$Rluc^N$ and $Rluc^C$-ER) in 12 well plates as described above. Four to six hours after transfection, cells were dissociated and re-plated into a 96-well plate (15,000 cells/well in 100 μl; white-wall plate, product no. 3610, Corning) coated with poly-D-lysine (50 μg/mL) and cultured overnight. Twenty-four hours post-

transfection, live cell substrate, EnduRen (30 μM, Promega), was added to the culture media and incubated for 2-5 hours. For drug treatment, indicated drug(s) was added together with EnduRen and 5 hours later luminescence was measured by a POLARstar Omega microplate reader (BMG LABTECH, Ortenberg, Germany).

Library screen

HEK293T cells cultured in 100 mm dish for 16 hours (with 75-80% confluency) were transfected with split-Rluc constructs (5 μg each). Four to six hours after transfection, cells were dissociated and plated onto 96-well plate (15,000 cells/well in 100 μl; white-wall plate, product no. 3610, Corning) coated with poly-D-lysine (50 μg/mL) and cultured for overnight. Twenty-four hours post-transfection, 1 μM of each compound (final concentration) was added to each well together with Enduren (30 μM, Promega). Plates were incubated at 37°C with 5% CO_2 for 5 hours and then luciferase activity (luminescence) was measured by a POLARstar Omega microplate reader (BMG LABTECH, Ortenberg, Germany). The split Rluc activity of each drug was normalized by quantile normalization (Bolstad et al. 2003) using R statistical software (version 4.0). After normalization, the average and the standard deviation (SD) of the control (DMSO treatment) were calculated. Potential hits were picked using the cut-off value of three times of SD (3SD) higher than the average of the control, and further tested for their activity with split-Rluc assay. Only the compounds that showed consistent increase (3 times higher than DMSO) were called as 'hits.' For drug enrichment analysis, we employed the over representation analysis (Boyle et al. 2004). False discovery rate (FDR) was calculated by R software. Circular packaging dendrogram were created using R version 4.0.0 with packages 'ggraph', 'igraph, 'tidyverse' and 'RcolorBrewer'.

Proximity labeling assay (PLA)

HeLa cells were transfected with SEC61-GFP expression vector (100ng) in 8 well chamber slide (Millipoer Sigma, Millicell EZ SLIDE) and, 16 hours post-transfection, treated with control (DMSO) or indicated drugs for 5 hours. Cells were fixed with 4% paraformaldehyde for 15 min and permeabilized with 0.5% Triton X-100 for 5min. Proximity ligation assay (PLA) was performed according to the manufacturer's recommendation (Duolink™ In Situ Red Starter Kit Mouse/Rabbit, Sigma-Aldrich). Primary antibodies against GFP (ab13970 from rabbit, Abcam) and Tom20 (sc-17764 from mouse, Santa Cruz Biotechnology) were used at 1:500 dilution each. After mounting, the images were captured by Zeiss Observer Z1 inverted microscope equipped with a Hamamatsu ORCA-Flash4.0 camera using Zeiss Zen Pro software. The image is analyzed in ImageJ with Maxima function. Number of PLA fluorescent puncta per cell was counted and averaged across multiple cells. For analyses, all PLA studies were internally compared.

Transmission Electron Microscopy (TEM)

HEK293T cells cultured in 100 mm dish with 90% confluency were treated with DMSO or isoproterenol for 30 min in the 37°C incubator with 5% CO_2. These monolayers of cells were fixed in the culture dish with glutaraldehyde/paraformaldehyde mixture (half-strength Karnovsky's fixative: 2g/dL paraformaldehyde, 2.5g/dL glutaraldehyde in 0.1M cacodylate buffer) (Karnovsky 1965) and post-fixed in 2% aqueous OsO_4 in 0.2M S-collidine buffer, pH 7.4. The monolayers were scrapped off the plastic dish with a rubber spatula, pelleted in a micro-centrifuge, dehydrated in graded ethanol solutions, transitioned into propylene oxide, and infiltrated and embedded in epoxy resin (Poly-Bed 812; Polysciences, Inc.; Warrington PA).

One-micron thick sections were cut on an ultra-microtome and stained on the glass slide with 1g/dL toluidine blue in 1g/dL aqueous borax. Thin sections were mounted on 200 mesh copper grids and stained with saturated solution of uranyl acetate and 0.4g/dL alkaline lead citrate (Venable & Coggeshall 1965; Reynolds 1963). The stained grids were examined on a Jeol JEM-100CX electron microscope equipped with a digital camera. With randomly selected EM images, the distance between the outer mitochondrial membrane (OMM) and ER membrane was measured. If the distance (measured in Image J) was within 25 nm, it was counted as 'contact', whereas if it was greater than 25 nm, 'no contact'. The number of mitochondria with ER contact was counted and its percentage over the total number of mitochondria was calculated.

Calcium level measurement

To monitor the mitochondrial calcium dynamics, mito-R-GECO1 construct (100 ng each) was transfected into HeLa cells plated in the 8 well chamber slide (Nunc, Lab-Tek II). Sixteen hours after transfection, the cells were treated with DMSO or indicated drugs for 4 hours and were imaged on Zeiss Observer Z1 inverted microscope equipped with a Zeiss incubator system and a Hamamatsu ORCA-Flash4.0 camera. Images were acquired using Zeiss Zen Pro software, every 2.5 sec for a duration of 5 min. Approximately 7.5 sec after the start of the experiment, histamine was superfused to transfected cells. For excitation of mito-R-GECO1, 535/40 nm filter was used; the emission filter was 624/40 nm. The boundary of each cell was set as ROIs (region of interest) and selected based on the presence of R-GECO1 fluorescent signal. $\Delta F/F_0$ was calculated as $(F-F_0)/F_0$, where F is fluorescence intensity of indicated fluorophore and F_0 is the baseline fluorescence intensity averaged over a 2.5-s period (during the control period) immediately

before the start of histamine stimulation. The mitochondrial Ca^{2+} uptake rate was calculated as $(\Delta F/F_0)/\Delta t$ (R-GECO1) as described previously (Fülöp et al. 2011).

Mitochondrial transmembrane potential measurements

Mitochondrial membrane potential (Ψ_{mit}) was measured by tetramethyl rhodamine methyl ester (TMRM) fluorescent dye (I34361, Thermo Fisher Scientific). HeLa cells were loaded with 10 nM TMRM for 30 min at RT and then treated with DMSO or isoproterenol for 1 hour. TMRM fluorescence was imaged using an inverted microscope Zeiss Observer Z1 inverted microscope equipped with a Hamamatsu ORCA-Flash4.0 camera using Zeiss Zen Pro software, and analyzed in Image J.

Mitochondrial DNA content measurement

DNAs were isolated from the HEK293T cells treated with DMSO or isoproterenol overnight, quantified, and used for real time PCR using mitochondrial DNA specific (tRNA-Leu (UUR)) primer sets (Forward, 5'- CAC CCA AGA ACA GGG TTT GT-3'; Reverse, 5'- TGG CCA TGG GTA TGT TGT TA-3') as well as nuclear DNA specific (B2-microglobulin) pirmer sets (Forward, 5'- TGC TGT CTC CAT GTT TGA TGT ATC T-3'; Reverse, 5'- TCT CTG CTC CCC ACC TCT AAG T-3'), as described previously (Rooney et al. 2015).

Statistical analysis

All statistical analyses were conducted in GraphPad Prism (version 8.4.2) or R (version 4.0.0), and *p* values were determined by paired two-tailed *t*-test, or unpaired two-tailed *t*-test with Welch's correction unless mentioned otherwise. All bar graphs are plotted as mean ± standard

error of measurement (SEM). All scattered plots are marked with individual data points and median value.

Acknowledgement

This work was supported by the National Institute of Neurological Disorders and Stroke (R01NS100007). The authors are grateful to Dr Jeffrey A. Golden and his lab members (Brigham and Women's Hospital/Harvard Medical School) for critical review of the manuscript, to Drs Sean E. Lawler and Michal Oscar Nowicki (Brigham and Women's Hospital/Harvard Medical School) for sharing their reagents and equipment, and to Amanda Frischmann for her assistance on compound list curating process.

Conflict of interest

The authors declare that they have no conflicts of interest with the contents of this article

REFERENCES

Area-Gomez, E. et al., 2012. Upregulated function of mitochondria-associated ER membranes in Alzheimer disease. *The EMBO journal*, 31(21), pp.4106–4123.

Balaban, R.S., 2009. The role of Ca(2+) signaling in the coordination of mitochondrial ATP production with cardiac work. *Biochimica et biophysica acta*, 1787(11), pp.1334–1341.

Barazzuol, L. et al., 2020. PINK1/Parkin Mediated Mitophagy, Ca2+ Signalling, and ER-Mitochondria Contacts in Parkinson's Disease. *International Journal of Molecular Sciences*, 21(5), 1772. doi:10.3390/ijms21051772

Billington, C.K., Penn, R.B. & Hall, I.P., 2017. β2 Agonists. *Handbook of experimental pharmacology*, 237, pp.23–40.

Bolstad, B.M. et al., 2003. A comparison of normalization methods for high density oligonucleotide array data based on variance and bias. *Bioinformatics*, 19(2), pp.185–193.

Booth, D.M. et al., 2016. Redox Nanodomains Are Induced by and Control Calcium Signaling at the ER-Mitochondrial Interface. *Molecular cell*, 63(2), pp.240–248.

Boyle, E.I. et al., 2004. GO::TermFinder--open source software for accessing Gene Ontology information and finding significantly enriched Gene Ontology terms associated with a list of genes. *Bioinformatics*, 20(18), pp.3710–3715.

Böckler, S. & Westermann, B., 2014. Mitochondrial ER contacts are crucial for mitophagy in yeast. *Developmental cell*, 28(4), pp.450–458.

Bravo, R. et al., 2011. Increased ER-mitochondrial coupling promotes mitochondrial respiration and bioenergetics during early phases of ER stress. *Journal of cell science*, 124(Pt 13), pp.2143–2152.

Calì, T. et al., 2012. α-Synuclein controls mitochondrial calcium homeostasis by enhancing endoplasmic reticulum-mitochondria interactions. *The Journal of biological chemistry*, 287(22), pp.17914–17929.

Cárdenas, C. et al., 2010. Essential regulation of cell bioenergetics by constitutive InsP3 receptor Ca2+ transfer to mitochondria. *Cell*, 142(2), pp.270–283.

Chakrabarti, R. et al., 2018. INF2-mediated actin polymerization at the ER stimulates mitochondrial calcium uptake, inner membrane constriction, and division. *The Journal of cell biology*, 217(1), pp.251–268.

Chen, T.-W. et al., 2013. Ultrasensitive fluorescent proteins for imaging neuronal activity. *Nature*, 499(7458), pp.295–300.

Cho, I.-T. et al., 2017. Ascorbate peroxidase proximity labeling coupled with biochemical fractionation identifies promoters of endoplasmic reticulum-mitochondrial contacts. *The Journal of biological chemistry*, 292(39), pp.16382–16392.

Ciccarelli, M. et al., 2013. Adrenergic receptors and metabolism: role in development of cardiovascular disease. *Frontiers in physiology*, 4, p.265.

Csordás, G., Weaver, D. & Hajnóczky, G., 2018. Endoplasmic Reticulum-Mitochondrial Contactology: Structure and Signaling Functions. *Trends in Cell Biology*, 28(7), pp.523–540.

de Brito, O.M. & Scorrano, L., 2008. Mitofusin 2 tethers endoplasmic reticulum to mitochondria. *Nature*, 456(7222), pp.605–610.

de Rooij, J. et al., 1998. Epac is a Rap1 guanine-nucleotide-exchange factor directly activated by cyclic AMP. *Nature*, 396(6710), pp.474–477.

Denton, R.M., 2009. Regulation of mitochondrial dehydrogenases by calcium ions. *Biochimica et biophysica acta*, 1787(11), pp.1309–1316.

Doghman Bouguerra, M. & Lalli, E., 2019. ER-mitochondria interactions: Both strength and weakness within cancer cells. *Biochimica et biophysica acta. Molecular cell research*, 1866(4), pp.650–662.

Eisenberg-Bord, M. et al., 2016. A Tether Is a Tether Is a Tether: Tethering at Membrane Contact Sites. *Developmental cell*, 39(4), pp.395–409.

Filadi, R. et al., 2016. Presenilin 2 Modulates Endoplasmic Reticulum-Mitochondria Coupling by Tuning the Antagonistic Effect of Mitofusin 2. *CellReports*, 15(10), pp.2226–2238.

Filadi, R. et al., 2018. TOM70 Sustains Cell Bioenergetics by Promoting IP3R3-Mediated ER to Mitochondria Ca2+ Transfer. *Current biology : CB*, 28(3), pp.369–382.e6.

Friedman, J.R. et al., 2011. ER tubules mark sites of mitochondrial division. *Science (New York, NY)*, 334(6054), pp.358–362.

Fülöp, L. et al., 2011. The effect of OPA1 on mitochondrial Ca^{2+} signaling. B. Zhivotovsky, ed. *PLoS ONE*, 6(9), p.e25199.

Gelmetti, V. et al., 2017. PINK1 and BECN1 relocalize at mitochondria-associated membranes during mitophagy and promote ER-mitochondria tethering and autophagosome formation. *Autophagy*, 13(4), pp.654–669.

Giacomello, M. et al., 2010. Ca2+ hot spots on the mitochondrial surface are generated by Ca2+ mobilization from stores, but not by activation of store-operated Ca2+ channels. *Molecular cell*, 38(2), pp.280–290.

Giordano, F. et al., 2013. PI(4,5)P(2)-dependent and Ca(2+)-regulated ER-PM interactions mediated by the extended synaptotagmins. *Cell*, 153(7), pp.1494–1509.

Hamasaki, M. et al., 2013. Autophagosomes form at ER-mitochondria contact sites. *Nature*, 495(7441), pp.389–393.

Hedskog, L. et al., 2013. Modulation of the endoplasmic reticulum-mitochondria interface in Alzheimer's disease and related models. *Proceedings of the National Academy of Sciences*, 110(19), pp.7916–7921.

Inoue, A. et al., 2019. Illuminating G-Protein-Coupling Selectivity of GPCRs. *Cell*, 177(7), pp.1933–1947.e25.

Ji, W.-K. et al., 2017. Receptor-mediated Drp1 oligomerization on endoplasmic reticulum. *The Journal of cell biology*, 216(12), pp.4123–4139.

Johnson, D.I., 1999. Cdc42: An essential Rho-type GTPase controlling eukaryotic cell polarity. *Microbiology and molecular biology reviews : MMBR*, 63(1), pp.54–105.

Joshi, A.U., Kornfeld, O.S. & Mochly-Rosen, D., 2016. The entangled ER-mitochondrial axis as a potential therapeutic strategy in neurodegeneration: A tangled duo unchained. *Cell Calcium*, 60(3), pp.218–234.

Karnovsky, M.J., 1965. A formaldehyde-glutaraldehyde fixative of high osmolality for use in electron microscopy. J. Cell Biol. 27:137-8A, 1965. *The Journal of cell biology*, (27), pp.137–8A.

Klecker, T., Böckler, S. & Westermann, B., 2014. Making connections: interorganelle contacts orchestrate mitochondrial behavior. *Trends in Cell Biology*, 24(9), pp.537–545.

Kornmann, B., 2013. The molecular hug between the ER and the mitochondria. *Current Opinion in Cell Biology*, 25(4), pp.443–448.

Kornmann, B. et al., 2009. An ER-mitochondria tethering complex revealed by a synthetic biology screen. *Science (New York, NY)*, 325(5939), pp.477–481.

Krols, M. et al., 2016. Mitochondria-associated membranes as hubs for neurodegeneration. *Acta Neuropathologica*, 131(4), pp.505–523.

Lang, A., Peter, A.T.J. & Kornmann, B., 2015. ER–mitochondria contact sites in yeast: beyond the myths of ERMES. *Current Opinion in Cell Biology*, 35, pp.7–12.

Lau, D.H.W. et al., 2018. Disruption of ER-mitochondria signalling in fronto-temporal dementia and related amyotrophic lateral sclerosis. *Cell Death and Disease*, 9(3), p.327.

Le Masson, G., Przedborski, S. & Abbott, L.F., 2014. A computational model of motor neuron degeneration. *Neuron*, 83(4), pp.975–988.

Lee, Seongsoo et al., 2016. Polo Kinase Phosphorylates Miro to Control ER-Mitochondria Contact Sites and Mitochondrial Ca(2+) Homeostasis in Neural Stem Cell Development., 37(2), pp.174–189.

Lee, Soyeon & Min, K.-T., 2018. The Interface Between ER and Mitochondria: Molecular Compositions and Functions. *Molecules and cells*, 41(12), pp.1000–1007.

Lim, Y. et al., 2015. Hereditary spastic paraplegia-linked REEP1 modulates endoplasmic reticulum/mitochondria contacts. *Annals of Neurology*, 78(5), pp.679–696.

Magistrelli, L. & Comi, C., 2020. Beta2-Adrenoceptor Agonists in Parkinson's Disease and Other Synucleinopathies. *Journal of neuroimmune pharmacology : the official journal of the Society on NeuroImmune Pharmacology*, 15(1), pp.74–81.

Mittal, N. et al., 2013. Select G-protein-coupled receptors modulate agonist-induced signaling via a ROCK, LIMK, and β-arrestin 1 pathway. *CellReports*, 5(4), pp.1010–1021.

Mittal, S. et al., 2017. β2-Adrenoreceptor is a regulator of the α-synuclein gene driving risk of Parkinson's disease. *Science (New York, NY)*, 357(6354), pp.891–898.

Moltedo, O., Remondelli, P. & Amodio, G., 2019. The Mitochondria-Endoplasmic Reticulum Contacts and Their Critical Role in Aging and Age-Associated Diseases. *Frontiers in Cell and Developmental Biology*, 7, p.172.

Moore, A.S. & Holzbaur, E.L.F., 2018. Mitochondrial-cytoskeletal interactions: dynamic associations that facilitate network function and remodeling. *Current Opinion in Psychology*, 3, pp.94–100.

Neumann, E., Khawaja, K. & Müller-Ladner, U., 2014. G protein-coupled receptors in rheumatology. *Nature reviews. Rheumatology*, 10(7), pp.429–436.

Ottolini, D. et al., 2013. The Parkinson disease-related protein DJ-1 counteracts mitochondrial impairment induced by the tumour suppressor protein p53 by enhancing endoplasmic reticulum-mitochondria tethering. *Human molecular genetics*, 22(11), pp.2152–2168.

Paillusson, S. et al., 2016. There's Something Wrong with my MAM; the ER-Mitochondria Axis and Neurodegenerative Diseases. *Trends in neurosciences*, 39(3), pp.146–157.

Perry, C.G.R. et al., 2013. Methods for assessing mitochondrial function in diabetes. *Diabetes*, 62(4), pp.1041–1053.

Peterson, L. et al., 2014. Potential benefits of therapeutic use of β2-adrenergic receptor agonists in neuroprotection and Parkinsonµs disease. *Journal of immunology research*, 2014, p.103780.

Phillips, M.J. & Voeltz, G.K., 2016. Structure and function of ER membrane contact sites with other organelles. *Nature reviews Molecular cell biology*, 17(2), pp.69–82.

Plenge-Tellechea, F., Soler, F. & Fernandez-Belda, F., 1997. On the inhibition mechanism of sarcoplasmic or endoplasmic reticulum Ca2+-ATPases by cyclopiazonic acid. *The Journal of biological chemistry*, 272(5), pp.2794–2800.

Qian, L. et al., 2011. β2-adrenergic receptor activation prevents rodent dopaminergic neurotoxicity by inhibiting microglia via a novel signaling pathway. *Journal of immunology*, 186(7), pp.4443–4454.

Reynolds, E.S., 1963. The use of lead citrate at high pH as an electron-opaque stain in electron microscopy. *The Journal of cell biology*, 17(1), pp.208–212.

Rieusset, J., 2018. The role of endoplasmic reticulum-mitochondria contact sites in the control of glucose homeostasis: an update. *Cell Death and Disease*, 9(3), p.388.

Rizzuto, R. et al., 1998. Close contacts with the endoplasmic reticulum as determinants of mitochondrial Ca2+ responses. *Science*, 280(5370), pp.1763–1766.

Rizzuto, R. et al., 1993. Microdomains with high Ca2+ close to IP3-sensitive channels that are sensed by neighboring mitochondria. *Science*, 262(5134), pp.744–747.

Rooney, J.P. et al., 2015. PCR based determination of mitochondrial DNA copy number in multiple species. *Methods in molecular biology*, 1241, pp.23–38.

Rowland, A.A. & Voeltz, G.K., 2012. Endoplasmic reticulum-mitochondria contacts: function of the junction. *Nature reviews Molecular cell biology*, 13(10), pp.607–625.

Scaduto, R.C. & Grotyohann, L.W., 1999. Measurement of mitochondrial membrane potential using fluorescent rhodamine derivatives. *Biophysj*, 76(1 Pt 1), pp.469–477.

Schon, E.A. & Area-Gomez, E., 2013. Mitochondria-associated ER membranes in Alzheimer disease. *Molecular and cellular neurosciences*, 55, pp.26–36.

Scorrano, L. et al., 2019. Coming together to define membrane contact sites. *Nature Communications*, 10(1), p.1287.

Shao, X. et al., 2015. Mechanical stimulation induces formin-dependent assembly of a perinuclear actin rim. *Proceedings of the National Academy of Sciences*, 112(20), pp.E2595–601.

Simmen, T. et al., 2005. PACS-2 controls endoplasmic reticulum-mitochondria communication and Bid-mediated apoptosis. *EMBO Journal*, 24(4), pp.717–729.

Sinha, S. & Yang, W., 2008. Cellular signaling for activation of Rho GTPase Cdc42. *Cellular signalling*, 20(11), pp.1927–1934.

Söderberg, O. et al., 2006. Direct observation of individual endogenous protein complexes in situ by proximity ligation. *Nature Methods*, 3(12), pp.995–1000.

Stoica, R. et al., 2016. ALS/FTD-associated FUS activates GSK-3β to disrupt the VAPB-PTPIP51 interaction and ER-mitochondria associations. *EMBO reports*, 17(9), pp.1326–1342.

Stoica, R. et al., 2014. ER-mitochondria associations are regulated by the VAPB-PTPIP51 interaction and are disrupted by ALS/FTD-associated TDP-43. *Nature Communications*, 5(1), p.3996.

Tambini, M.D. et al., 2016. ApoE4 upregulates the activity of mitochondria-associated ER membranes. *EMBO reports*, 17(1), pp.27–36.

Tepikin, A.V., 2018. Mitochondrial junctions with cellular organelles: Ca2+ signalling perspective. *Pflügers Archiv - European Journal of Physiology*, 470(8), pp.1181–1192.

Territo, P.R. et al., 2000. Ca(2+) activation of heart mitochondrial oxidative phosphorylation: role of the F(0)/F(1)-ATPase. *American journal of physiology. Cell physiology*, 278(2), pp.C423–35.

Vance, J.E., 2014. MAM (mitochondria-associated membranes) in mammalian cells: lipids and beyond. *Biochimica et biophysica acta*, 1841(4), pp.595–609.

Vance, J.E., 1990. Phospholipid synthesis in a membrane fraction associated with mitochondria. *The Journal of biological chemistry*, 265(13), pp.7248–7256.

Venable, J.H. & Coggeshall, R., 1965. A simplified lead citrate stain for use in electron microscopty. *The Journal of cell biology*, 25(2), pp.407–408.

Voeltz, G.K. et al., 2006. A class of membrane proteins shaping the tubular endoplasmic reticulum. *Cell*, 124(3), pp.573–586.

Watanabe, S. et al., 2016. Mitochondria-associated membrane collapse is a common pathomechanism in SIGMAR1- and SOD1-linked ALS. *EMBO molecular medicine*, 8(12), pp.1421–1437.

Wu, J. et al., 2013. Improved orange and red $Ca^{2}\pm$ indicators and photophysical considerations for optogenetic applications. *ACS chemical neuroscience*, 4(6), pp.963–972.

Yi, M., Weaver, D. & Hajnóczky, G., 2004. Control of mitochondrial motility and distribution by the calcium signal: a homeostatic circuit. *The Journal of cell biology*, 167(4), pp.661–672.

Zampese, E. et al., 2011. Presenilin 2 modulates endoplasmic reticulum (ER)-mitochondria interactions and Ca2+ cross-talk. *Proceedings of the National Academy of Sciences*, 108(7), pp.2777–2782.

Zhao, Y. et al., 2011. An expanded palette of genetically encoded Ca^{2+} indicators. *Science*, 333(6051), pp.1888–1891.

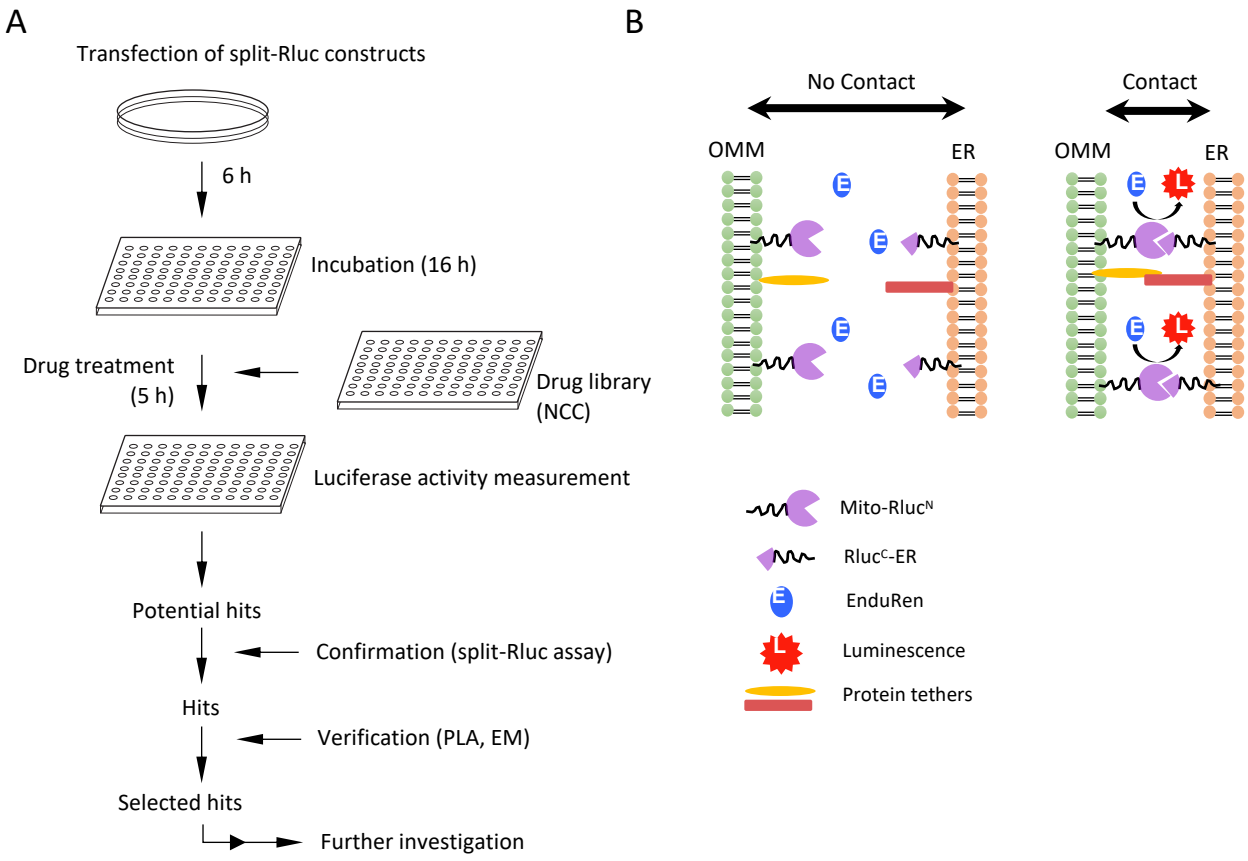

Figure 1. Drug screening with split-Rluc assay system. *A,* Schematic diagram showing a workflow of drug screening. EM, electron microscopy; NCC, NIH Clinical Collection; PLA, proximity ligase assay; Rluc, Renilla luciferase. *B,* Schematic diagram of split-Rluc assay system and its involved components (adapted from Cho *et al*., 2017). ER, endoplasmic reticulum; Mito-Rluc^{N}, N-terminal half of the Rluc with mitochondria targeting sequence; OMM, outer mitochondrial membrane; RlucC-ER, C-terminal half of the Rluc with ER targeting sequence.

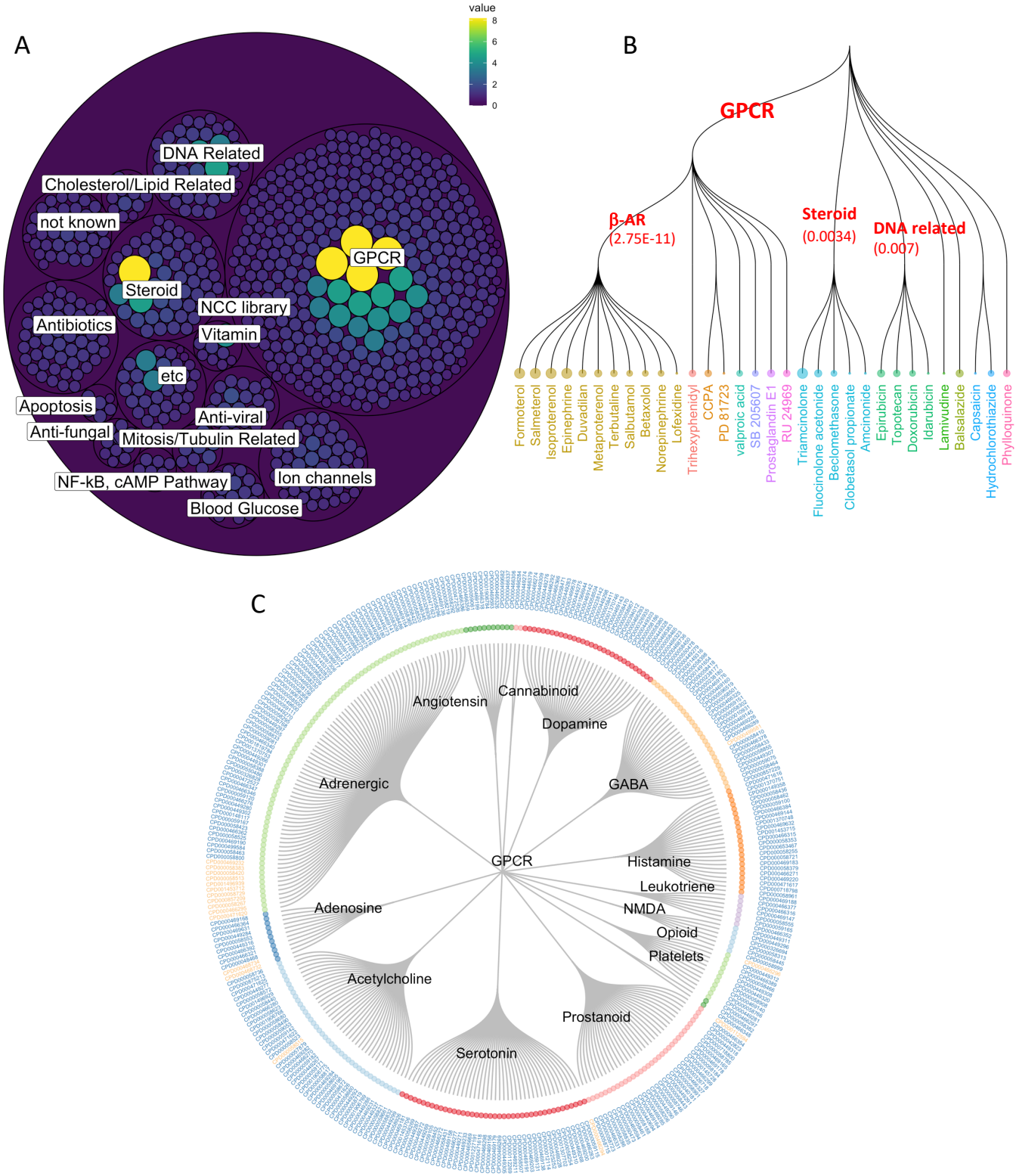

Figure 2. Screened compounds with their predicted target pathway. *A,* Circular packaging of NCC library drugs grouped with their predicted target pathway. Small circles represent each drug (the circle size corresponds to normalized split-Rluc activity (see color key) of each drug). Green to yellow circles indicate potential hits (cut off 3SD). The numbers in color key indicate x times SD. *B,* Dendrogram of 31 potential hits identified from the initial screen. Circle size indicates normalized split-Rluc activity of each drug. Numbers in the parenthesis indicate false discovery rate (adjusted *p* values). *C,* Circular dendrogram of all drugs targeting GPCR families sub-grouped into each GPCR pathway. Drug IDs with orange color represent 18 potential hits associated with GPCR pathways

A

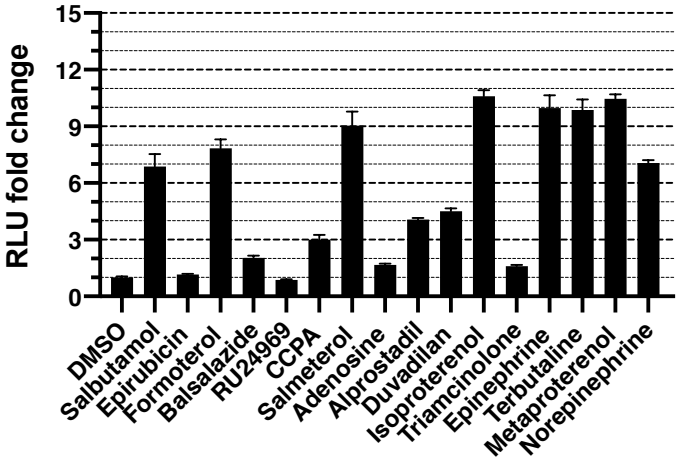

B

Structure_ID	Drug Name	Target GPCR	Receptor specificity	Fold change
CPD000058267	Isoproterenol	AR	beta	10.6
CPD001453712	Metaproterenol	AR	beta	10.5
CPD000857209	Epinephrine	AR	alpha, beta	10
CPD001496939	Terbutaline Sulfate	AR	beta-2	9.9
CPD000466295	Salmeterol	AR	beta-2	9.0
CPD000471620	Formoterol	AR	beta-2	7.8
CPD000058383	Norepinephrine	AR	alpha, beta	7.1
CPD000058513	Salbutamol	AR	beta-2	6.9
CPD000058729	Duvadilan	AR	beta	4.5
CPD000112594	Alprostadil (PGE1)	PGE2R	EP1, EP2	4.1
CPD000468732	CCPA	AdR	A1	3.0

C

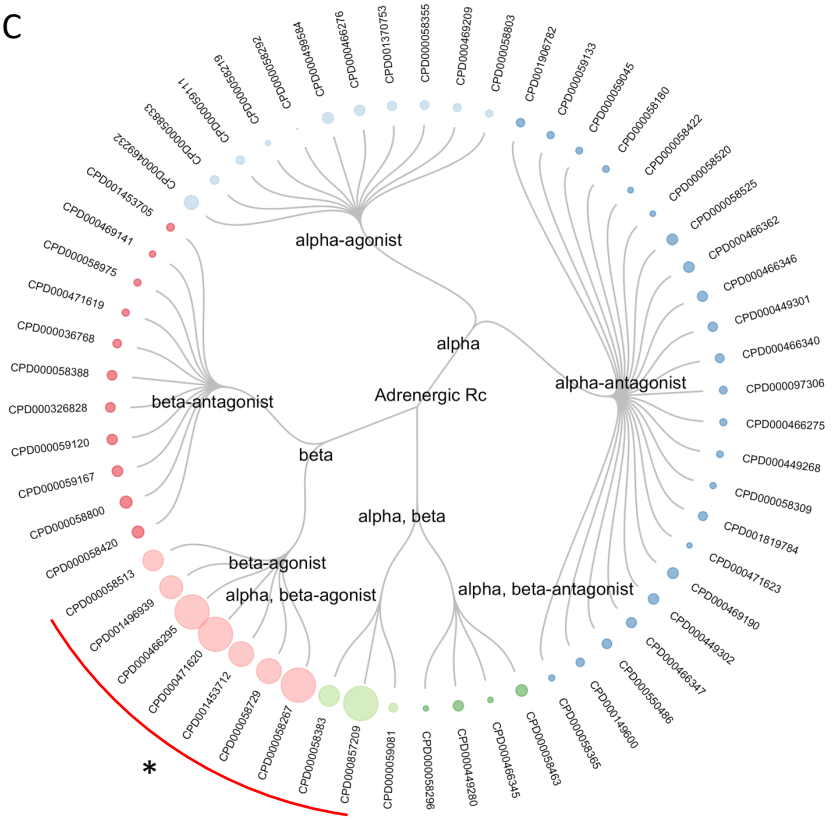

D

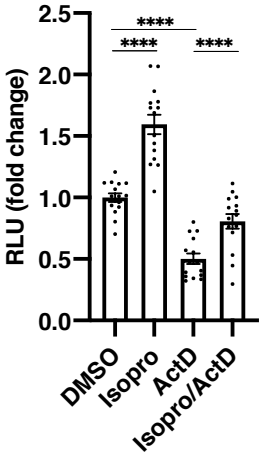

Figure 3. GPCR agonists are confirmed to increase split-Rluc activity. *A,* Split-Rluc assay results of the control (DMSO) and a subset of potential hits identified from the initial screen. Mean RLU (relative light unit) fold change is plotted for each drug (n = 3). *B*, A list of 11 confirmed hits that show 3 times or higher fold change (of each compound's split-Rluc activity compared to DMSO). AR: adrenergic receptor; AdR, adenosine receptor; CCPA, 2-chloro-N^{6}cyclopentyladenosine; PGE1, prostaglandin E1 (alprostadil is synthetic PGE1); PGE2R, PGE2 receptor. *C,* Circular dendrogram of all drugs targeting adrenergic receptors (ARs). Circle size represents normalized split-Rluc activity of each drug; circle color indicates target specificity. Nine hits are marked with red curve with asterisk (*). *D,* Split-Rluc assay in cells treated with DMSO, isoproterenol (isoprot), actinomycin D (ActD), or isoprot and ActD. Mean RLU (relative light unit) fold change is plotted for each condition (n = 15 wells each from 3 experiments; **** $p < 0.0001$; paired two-tailed t-test).

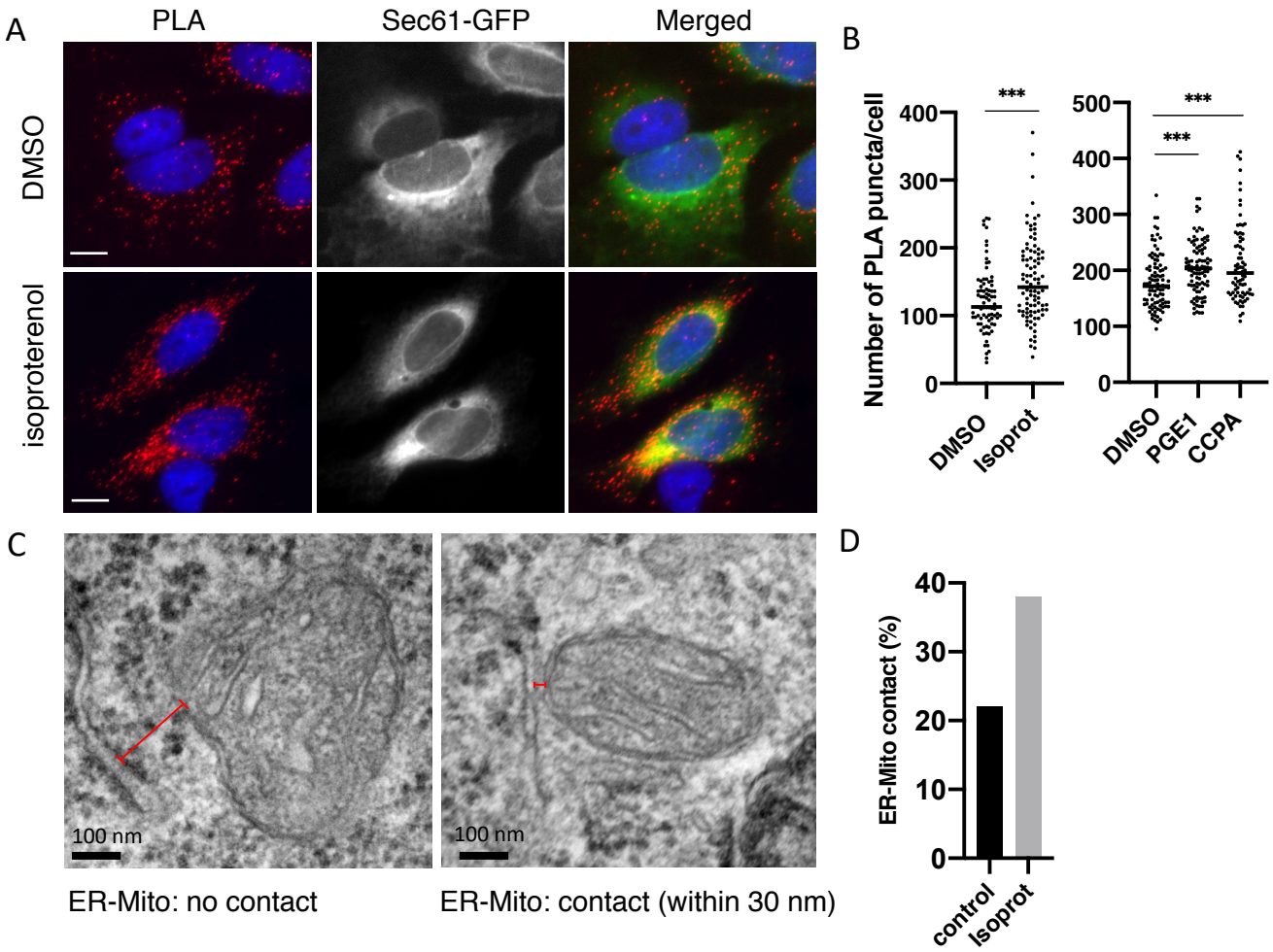

Figure 4. GPCR agonists enhance physical contact between ER and mitochondria. *A,* Representative images of *in situ* proximity ligation assay (PLA) in cells treated with DMSO (top) or isoproterenol (β-AR agonist) (bottom). PLA fluorescent signal (red) indicates a close apposition between ER and mitochondria. Sec61-GFP (green) was used to label ER and API (blue) was for nucleus. Arrows mark the cells transfected with Sec61-GFP in each channel. Scale bars: 10 μm. *B,* Quantification of *in situ* PLA from cells treated with DMSO, isoproterenol (isoprot), CCPA, and PGE1. Number of PLA puncta was counted in each cell and averaged across multiple cells (n = 81 and 93 cells for DMSO and isoprot; n = 97, 96, and 77 cells for DMSO, PGE1, CCPA; p = 0.0003, 0.003, and 0.0008 for isoprot, PGE1, CCPA; unpaired two-tailed t-test with Welch's correction). *C,* Representative transmission electron micrographs showing examples of mitochondria that was counted as the one with a close contact (right) or no contact (left) with ER membrane. Red line depicts the distance measured between the outer mitochondrial membrane (OMM) and ER membrane. Scale bars: 100 nm. *D,* Quantification of the percentage of ER-Mito contact in control vs isoproterenol treated cells (n = 59, 63 mitochondria for control, isoprot).

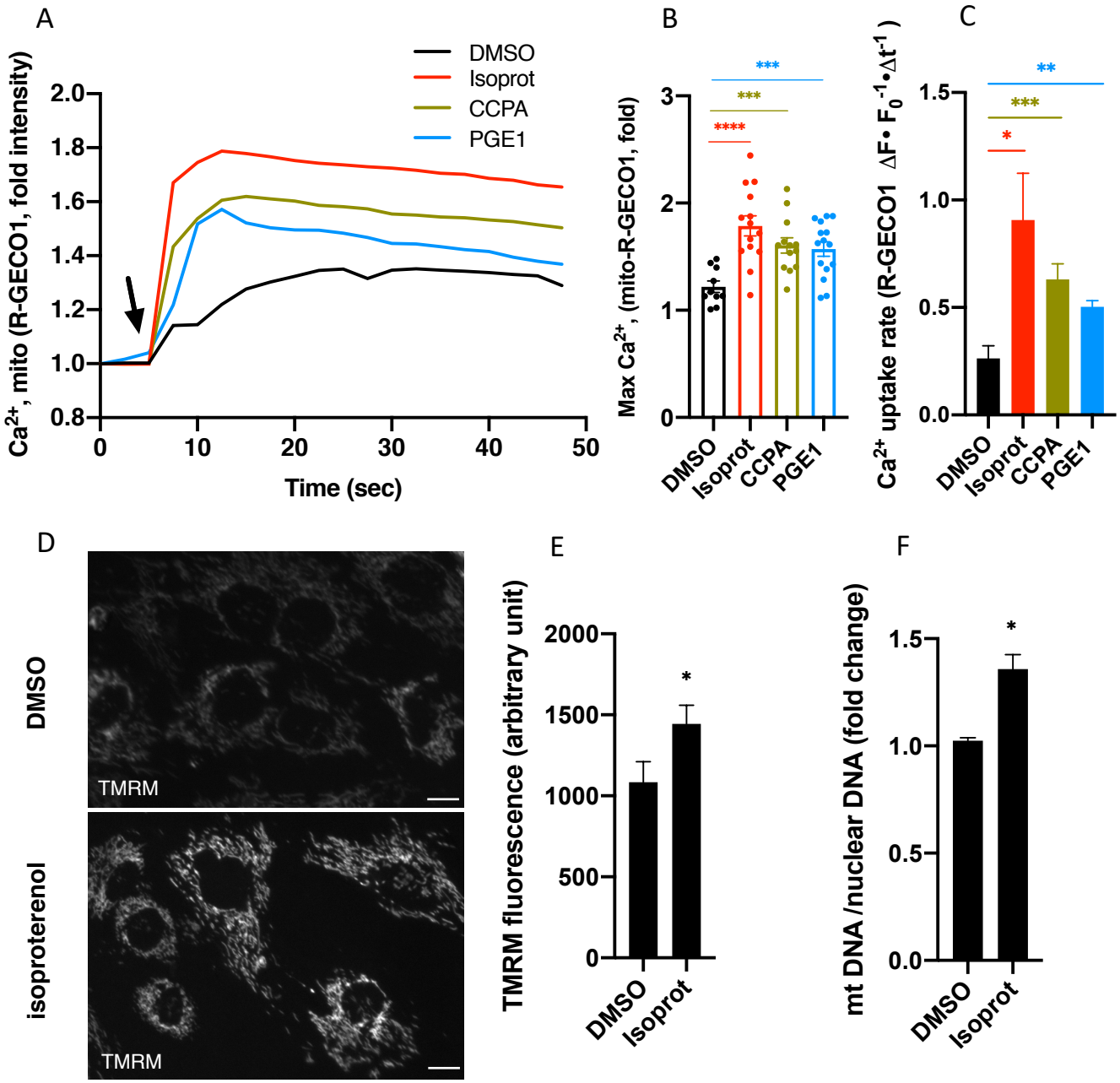

Figure 5. GPCRs enhance mitochondrial Ca^{2+} uptake. *A,* Mitochondrial Ca^{2+} uptake in HeLa cells treated with DMSO, CCPA, isoproterenol (isoprot), or PGE1, in response to ER Ca^{2+} release triggered by histamine. Mito-R-GECO1 fluorescent intensity change ($\Delta F/F_0$) averaged across multiple neurons is plotted for each drug (n = 10, 14, 13, and 15 cells for DMSO, isoprot, CCPA, and PGE1, from 3 experiments) every 2.5 sec after adding histamine (arrow indicates when histamine was added). *B,* Maximum peak mitochondrial Ca^{2+} uptake for each drug. Maximum mito-R-GECO1 fluorescent intensity change ($\Delta F/F_0$) averaged across multiple neurons was normalized to that of DMSO and plotted as the fold change (from the same experiments in A) ($p < 0.0001$, p = 0.0003, 0.0004 for isoprot, CCPA, and PGE1; unpaired two-tailed t-test with Welch's correction). *C,* Mitochondrial Ca^{2+} uptake rate for each drug (from the same experiments in A) (p = 0.0151, 0.0006, and 0.0019 for isoprot, CCPA, and PGE1; unpaired two-tailed t-test with Welch's correction). *D,* Representative images of TMRM fluorescent signal in HeLa cells treated with control or isoprot. Scale bars: 10 µm. E, Quantification of TMRM fluorescence (n = 20, DMSO; n = 15, isoprot; p = 0.0436; unpaired two-tailed t-test with Welch's correction). F, Quantification of mitochondrial (mt) DNA content. The relative ratio of mtDNA fluorescent intensity over nuclear DNA is plotted (n = 3; p = 0.0334 ; unpaired two-tailed t-test with Welch's correction). All data expressed as mean +/- SEM)

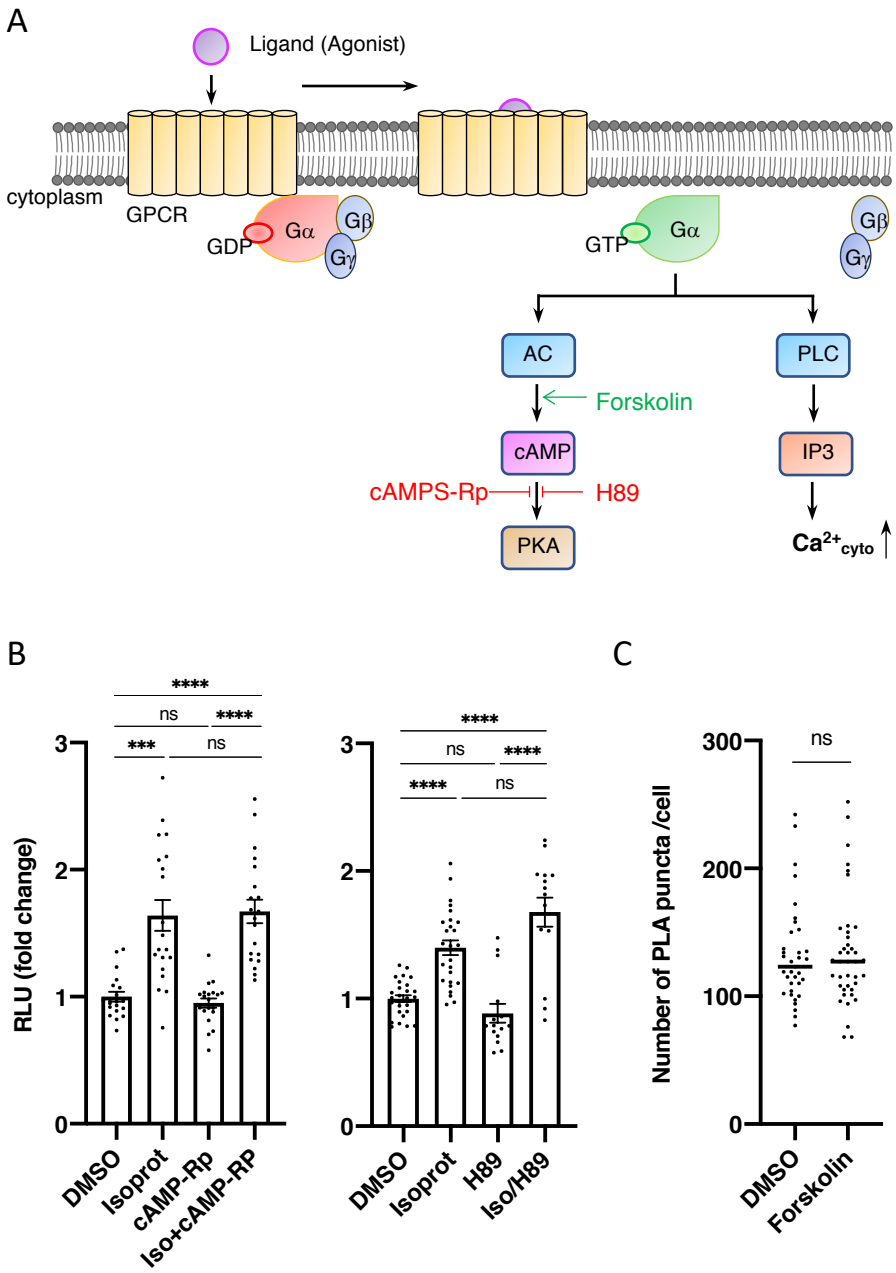

Figure 6. Inhibition of cAMP/PKA pathway does not suppress the effect of b-AR agonist on ER-Mito contact. *A*, Schematic diagram illustrating downstream effectors of the GPCR pathway. AC: adenylate cyclase; G_α, G_β, and G_γ: α, β, and γ subunits of G-protein; PKA: protein kinase A; PLC: phospholipase C. Forskolin is an activator of AC; cAMPS-Rp and H89 are inhibitors of PKA. *B,* Split-Rluc activity in DMSO- or indicated drug- treated cells (n = 20 wells each from 3 experiments; ***$p < 0.001$, ****$p < 0.0001$, ns = not significant; paired two-tailed *t*-test). *C,* Quantification of *in situ* PLA in DMSO or forskolin treated cells (n = 35, DMSO; n = 40, forskolin; unpaired two-tailed *t*-test with Welch's correction).

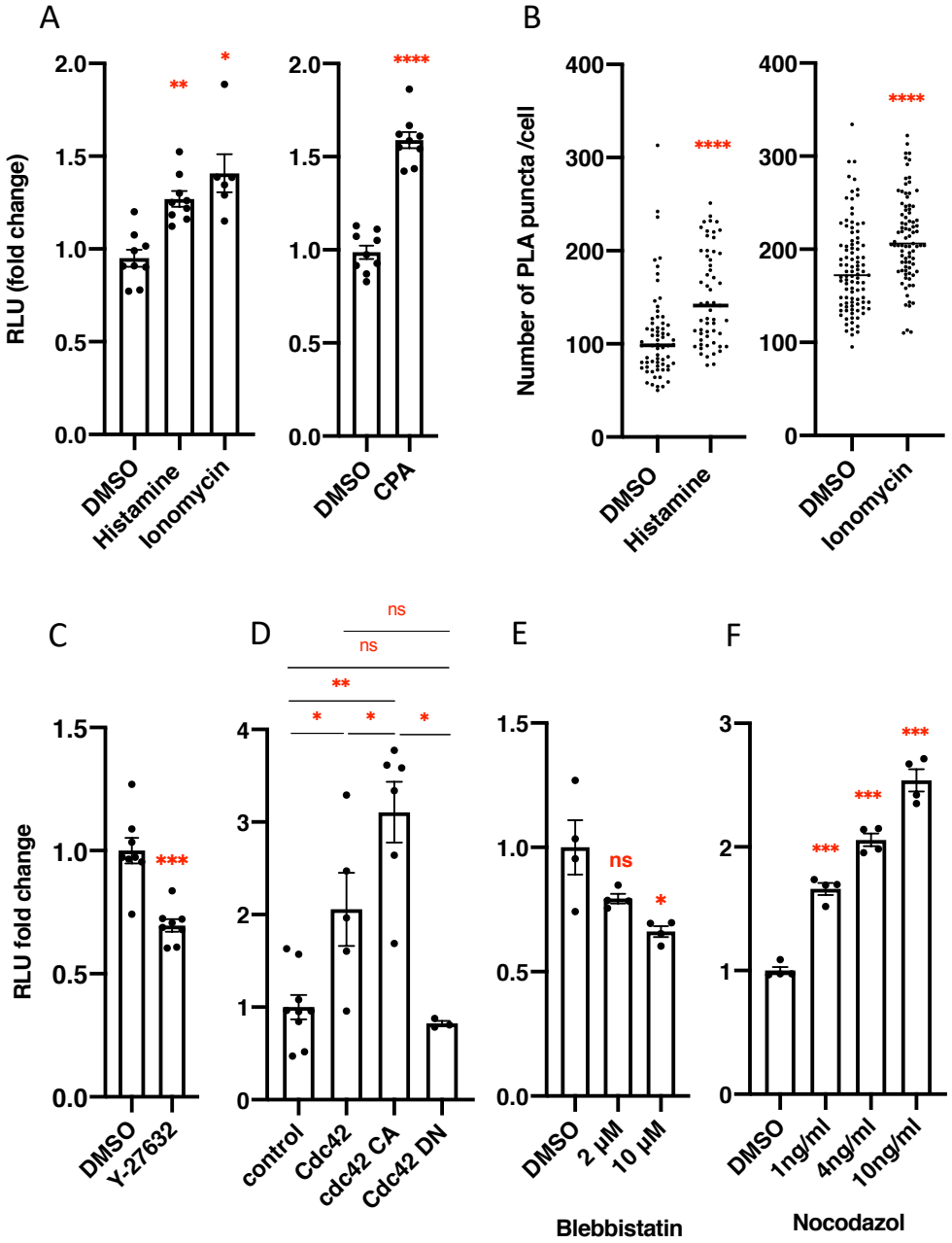

Figure 7. Elevated cytosolic Ca^{2+} level enhances ER-Mito contact. *A,* Split-Rluc activity in DMSO, histamine, ionomycin, or CPA treated cells (n = 9 wells, DMSO, histamine, and CPA; n = 6, ionomycin; **p = 0.0017, *p = 0.0256, ****p < 0.0001; paired t-test). *B,* Quantification of *in situ* PLA (n = 66, 57, 97, 87 cells for DMSO, histamine, DMSO, ionomycin;****p < 0.0001;). *C,* Split-Rluc activity of the cells treated with DMSO or Y-27632 (ROCK inhibitor). n = 8 wells for DMSO and Y-27632; ***p = 0.0046; t-test. *D,* Split-Rluc activity of the cells transfected with control vector (n = 9 wells), wild type (WT) Cdc42 (n = 5), constitutively active (CA) Cdc42 (n = 6), or dominant negative (DN) Cdc42 (n = 3). * p < 0.05, **p = 0.0007, ns = not significant; paired t-test. *E-F,* Split-Rluc activity of the cells treated with different doses of blebbistatin (myosin II inhibitor) (E) or nocodazole (tubulin inhibitor) (F) compared to DMSO treated (n = 4; ***p < 0.001; paired t-test)